EUROPEAN ORGANIZATION FOR NUCLEAR RESEARCH

CERN/SPS/80-7/DI (LTD)

A COMPUTER SIMULATION OF INJECTION INTO A SUPERCONDUCTING PROTON RING

Chen Bofei*, Chen Siyu*, E.J.N. Wilson

Abstract

As part of the CERN-DESY collaboration on the design of the HERA project, we report computer simulation of injection dynamics in a superconducting proton ring. The effect of persistent current sextupole fields must clearly be carefully minimised if particle losses are to be avoided.

Geneva
June 1980

* Visitors from Institute of High Energy Physics, Beijing, People's Republic of China.

1. INTRODUCTION

Experience with the large proton machines at FNAL[1] and the SPS[2] shows that it is by no means easy to tune the machine to avoid particle loss at injection field. Conventional dipole magnets have a significant sextupole component in their remanent field pattern which as well as exciting third order resonances can drive half integer and coupling resonances if the closed orbit of the machine is not perfect. Tuning the machine to correct the orbit, reduce the Q spread by chromaticity compensation and steer away from non-linear resonances in the Q diagram is a delicate procedure but must be perfected if the life-time of the injected beam is to be more than a few seconds.

Turning to superconducting proton rings like the FNAL Energy Doubler[3] or the proton ring of the electron-proton proposal HERA[4] at DESY the injection field problems become even more serious. The sextupole components formed by persistent currents flowing in the superconductor are between one and two orders of magnitude stronger than the remanent sextupole of present day room temperature machines. In the case of the energy doubler this may be largely offset by injecting at 150 GeV instead of at the 8 GeV level used for the main ring, but in HERA's case the injection energy is the limited to the 40 GeV top energy of PETRA's magnet ring which will be used as a proton injector. However by using a higher Q for HERA, the sensitivity of the machine to sextupole fields at 40 GeV may well be no worse than the energy doubler at 150 GeV. On the other hand HERA must wait 15 minutes or so at this low field while proton bunches are injected so that no losses may be tolerated.

In this report we describe a study of the effect of persistent current sextupole fields on the dynamics of HERA. Analytic theory is compared with the results of particle simulation using the program LIMATRA. The studies confirm that the persistent current severely restrict the range of Q values which are stable and place critical tolerances on the correction of orbits and chromaticity. Beam dynamics simulation is restricted by the speed of contemporary computers to a study of the first few tens of milliseconds in the history of a hundred injected particles. Foreseeable improvements in speed could not extend this to match the 15 minutes or so life-time required of the real beam. However, in spite of this limitation we at least can place upper limits on the tuning range and establish pointers towards better machine design.

2. THE LATTICE AND OTHER MACHINE PARAMETERS

Table 1 lists the parameters of the rather early version of the HERA lattice used for this study. More recent versions differ in that vertical bends are introduced at the four insertions, the matching of the four low beta insertions, and the phase advance per normal period are somewhat different. Nevertheless, as an example of a 6 km circumference proton machine with four low beta insertions lattice used is a sufficiently representative approximation for our purposes. Figure 1 shows the low beta insertion and Figure 2 gives an overall picture of the machine.

The Q of the lattice has been chosen to be just that used in the SPS. It is about six integers higher than the FNAL main ring and Energy Doubler.

3. THE EFFECT OF PERSISTENT CURRENTS

We take our information on measurements of sextupole field due to persistent current from the Fermilab Energy Doubler Design Report [3]. Since we are unsure how to scale the effect with magnet aperture or filament diameter we assume these parameters will be the same for both HERA and the energy doubler. The HERA proposal actually quotes a somewhat larger bore magnet but this will not significantly affect our conclusions.

3.1. Persistent Currents

Fig. 3 from Ref. shows the measured persistent sextupole term as a function of excitation. The curve is displaced upward by a geometric sextupole which we remove from our calculations. We assume the magnet current is reduced below the injection level somewhat and then brought up to 200 A injection value to avoid a rapid transition from the upper to lower branch of the curve at the beginning of acceleration. The current of 200 A is 1/20th of the excitation peak and corresponds in the HERA case to 40 GeV/c. We find a sextupole error of

$$\frac{\Delta B}{B} = b_2 = -0.31 \times 10^{-3} \quad \text{at 1 cm}$$

or

$$K' = B''/B\rho = -0.0107\ m^{-3} .$$

Table 1 : HERA Lattice Parameters

Energy	(GeV)	840
Circumference	(m)	6451.2
Number of superperiods		4
Lattice		FODO
Straight section length	(m)	360
Number of cells		80
Cell length	(m)	62.64
Number of cell dipoles		640
Number of quadrupoles		160
Magnetic length of dipole	(m)	5.6886
Bending field	(Tesla)	4.83563
Bending angle	(mrad)	9.8175
Bending radius	(m)	579.436
Magnetic length of quad.	(m)	1.8
Transition γ_t		19.2025
Working point Q_x/Q_z		26.55/26.60
Nominal phase advance per cell	(^{o})	120
Cell quad. strength K_F/K_D	(m^{-2})	-0.02366/0.02707
Cell quad. gradient B'_F/B'_D	(Tesla/m)	66.361/-75.945
Cell beta function $\beta_x$max/$\beta_x$min	(m)	111.57/22.38
Cell beta function $\beta_z$max/$\beta_x$min	(m)	104.104/16.02
Cell dispersion D_{max}/D_{min}	(m)	4.29/2.12
Emittance $\varepsilon_x/\varepsilon_z$*	(πmm.mrad)	0.4585/0.22925
Injection energy	(GeV)	40

* $\varepsilon = \sigma^2/\beta$ at injection energy of 40 GeV

This represents a $B''/B\rho$ which is about 18 times that in an average CERN SPS magnet at injection [5], the SPS being a machine of comparable size and dynamical properties.

3.2. Chromaticity from Persistent Currents and its Correction

We define and calculate the chromaticity :

$$\xi = \frac{P}{Q}\,\frac{\partial Q}{\partial P} = \frac{1}{4\pi\, Q}\oint K'(s)\,\beta(s)\,D_x(s)\,ds \qquad (1)$$

It can be seen from this expression that machines which have a high Q, and hence also a low β and D_x, will have a small chromaticity for a given energy and sextupole error. This reduction in sensitivity to sextupole error is a strong argument for a high working point. In retrospect it explains why the SPS, with a Q of about 27, is three times less sensitive to sextupole than the Fermilab main ring. We have chosen a Q value close to 27 for HERA in order to take advantage of this factor 3 and, we hope, largely counterbalance the low 40 GeV injection energy.

We have used the program AGS to compute the chromaticity with and without sextupole fields and to compute sextupole strength necessary to cancel these chromaticities.

For this calculation we assume a simple pattern of sextupoles, one family close to F quadrupoles (SF) and one family close to D quadrupoles (SD). Each family has 80 sextupoles 50 cm long. Table 2 shows the results of these calculations. Lines A and B would apply at high energy if persistent currents had no effect, while lines C and D include the combined effect of natural and persistent chromaticity at 40 GeV.

Table 2 Chromaticity and Corrector Strength

	K' (m^{-3})			ξ_H	ξ_V
	$\frac{B''}{B\rho}$	SF (ℓ = 0.5 m)	SD (ℓ = 0.5 m)		
A	0.0	0.0	0.0	- 2.91	- 2.65
B	0.0	- 0.0721	0.1359	0.0	0.0
C	- 0.0107	0.0	0.0	16.58	- 17.08
D	- 0.0107	0.2633	0.63907	0.0	0.0

In order to reduce the correction to be applied by these sextupoles we propose to build the dipole magnets with a certain geometric sextupole bias. There will be two kinds, those placed near horizontally focusing quadrupoles, and those near defocusing quadrupoles. Together they will ensure a net chromaticity at high energy which is close to zero. This leaves the correction sextupoles to trim the chromaticity to be negative or positive according to the dictates of instability suppression.

4. ANALYTIC CALCULATION OF STOP-BAND WIDTH

Our analysis is intended to reveal the mechanism of stop-band excitation rather than provide a substitute for generally accepted and rigorous expressions for stop-band width. Fig. 4 shows diagramatically the model of the effect of a sextupole (assumed to lie at a maximum value of β). One finds the mean phase advance per turn is shifted by :

$$\Delta Q_x = \int_0^{2\pi} \frac{R\,\beta_x(\theta)}{4\pi a_x(\theta)}\, K'(\theta) \Big\{ \Big[\big(a_x(\theta)\cos Q_x\theta + d_x(\theta) \big)^2 - \big(a_z(\theta)\cos Q_z\theta + d_z(\theta) \big)^2 \Big] \cos Q_x\theta \Big\} d\theta \qquad (2)$$

$$\Delta Q_x = \int_0^{2\pi} \frac{R\beta_z(\theta)}{2\pi a_z(\theta)}\, K'(\theta) \Big\{ \big[a_x(\theta)\cos Q_x\theta + d_x(\theta) \big] \big[a_z(\theta)\cos Q_z\theta + d_z(\theta) \big] \cos Q_z\theta \Big\} d\theta \qquad (3)$$

where $a_x(\theta) = \sqrt{\varepsilon_x \beta_x(\theta)}$

$a_z(\theta) = \sqrt{\varepsilon_z \beta_z(\theta)}$

$d_x(\theta)$ and $d_z(\theta)$ are the closed orbit distortion in horizontal and vertical planes respectively

R is the mean radius

We expand the terms in curly brackets in the integral into :

$$\tfrac{1}{4} a_x^2 \cos 3Q_x\theta + a_x d_x \cos 2Q_x\theta + (d_x^2 - d_z^2 + \tfrac{3}{4}a_x^2 - \tfrac{1}{2}a_z^2) \cos Q_x\theta + a_x d_x - \tfrac{1}{4} a_z^2 \left[\cos(2Q_z+Q_x)\theta + \cos(2Q_z-Q_x)\theta \right] - a_z d_z \left[\cos(Q_z+Q_x)\theta + \cos(Q_z-Q_x)\theta \right] \qquad (4)$$

$$\tfrac{1}{2} a_z d_x \cos 2Q_z\theta + d_x d_z \cos Q_z\theta + \tfrac{1}{2} a_x a_z \cos Q_x\theta + \tfrac{1}{2} a_z d_x + \tfrac{1}{4} a_x a_z \left[\cos(2Q_z+Q_x)\theta + \cos(2Q_z-Q_x)\theta \right] + \tfrac{1}{2} a_x d_z \left[\cos(Q_z+Q_x)\theta - \cos(Q_z-Q_x)\theta \right] \qquad (5)$$

finding the angles characteristic of three third order resonances, four second order resonances, the difference coupling resonance, two integer resonances and a beam tune shift.

We next express the amplitudes a_x, a_z in terms of the beta functions and the beam emittances and treat each frequency as a term in a Fourier analysis of the sextupole pattern, appropriately weighted with a function of beta around the ring.

Only one term in the Fourier series : that corresponding to the closest stop-band of each type is important and these coefficients together with the stop-bands and expressions for widths they define are listed in Table 3.

We see that the resonances excited reflect those listed in Expressions 2 & 3.They include systematic third order resonances $3Q_x = 80$, $2Q_z + Q_x = 80$ and the difference resonances $2Q_z - Q_x = 27$, which are all independent of closed orbit errors.

The second order resonances $2Q_x = 53$, $2Q_z = 53$, $Q_x+Q_z = 53$ and the coupling resonance $Q_x-Q_z = 0$ are all driven by closed orbit effects. The nearest horizontal integer has four driving terms, two of which are orbit dependent, and there is a constant Q shift which is orbit dependent.

Of course a particular distribution of random orbit errors at each sextupole was used to compute those coefficients which depend on distortion. The rms value of this distortion was 4 mm in each plane. The conventional 98% expectation value of each coefficient would be twice as large as we have quoted and the coefficients can be scaled to other rms values of the distortion with the appropriate dependence on $d_{x,z}$.

5. PARTICLE TRACKING WITH LIMATRA

The program LIMATRA [6] tracks single particles or groups of particles distributed in six dimensional phase space around a synchrotron noting when individual particles leave the vacuum chamber of the machine. At the end of a specified number of turns, particle coordinates or phase space distributions are printed to see if surviving particles have departed from ideal linear motion.

The synchrotron model comprises a sequence of non-linear magnetic elements each with a value of β, α, η and betatron phase in each plane for the synchronous ($\Delta p/p = 0$) particle which is transferred directly from AGS [7]. In this simulation study these elements were the sextupoles, one

Table 3 : Analytic Calculation of Resonances Excited by Persistent Currents at 40 GeV

Order	The Coefficient of Fourier Series		Half Stop-band Width	
	Expression	Value	Expression	Value
$3Q_x=80$	$a_{80}=\frac{1}{\pi}\int_{-\pi}^{\pi}\beta_x^{3/2}k'\cos 80\theta\,d\theta$	-0.223	$\Delta Q_x=\frac{R}{16}\sqrt{\epsilon_x}\,a_{80}$	-9.7×10^{-3}
$2Q_x=53$	$a_{53}=\frac{1}{\pi}\int_{-\pi}^{\pi}\beta_x d_x k'\cos 53\theta\,d\theta$	-9.26×10^{-5}	$\Delta Q_x=\frac{R}{4}a_{53}$	-2.38×10^{-2}
$2Q_z=53$	$a_{53}=\frac{1}{\pi}\int_{-\pi}^{\pi}\beta_z d_x k'\cos 53\theta\,d\theta$	-6.12×10^{-5}	$\Delta Q_z=\frac{R}{4}a_{53}$	-1.57×10^{-2}
$Q_x=27$	$a_{27}=\frac{1}{\pi}\int_{-\pi}^{\pi}\beta_x^{1/2}d_x^2k'\cos 27\theta\,d\theta$	-6.8×10^{-9}	$\Delta Q_x=\frac{R}{4\sqrt{\epsilon_x}}a_{27}$	-2.6×10^{-3}
	$a_{27}=\frac{1}{\pi}\int_{-\pi}^{\pi}\beta_x^{1/2}d_z^2k'\cos 27\theta\,d\theta$	1.08×10^{-8}	$\Delta Q_x=-\frac{R}{4\sqrt{\epsilon_x}}a_{27}$	-4.1×10^{-3}
	$a_{27}=\frac{1}{\pi}\int_{-\pi}^{\pi}\beta_x^{3/2}k'\cos 27\theta\,d\theta$	-2.29×10^{-6}	$\Delta Q_x=\frac{3R}{16}\sqrt{\epsilon_x}\,a_{27}$	-3.0×10^{-7}
	$a_{27}=\frac{1}{\pi}\int_{-\pi}^{\pi}\beta_x^{1/2}\beta_z k'\cos 27\theta\,d\theta$	-3.0×10^{-6}	$\Delta Q_x=-\frac{R}{8}\frac{\epsilon_z}{\sqrt{\epsilon_x}}a_{27}$	1.3×10^{-7}
			$\Delta Q_z=\frac{R}{4}\sqrt{\epsilon_x}\,a_{27}$	-5.2×10^{-7}
$Q_z=27$	$a_{27}=\frac{1}{\pi}\int_{-\pi}^{\pi}\beta_z^{1/2}d_x d_z k'\cos 27\theta\,d\theta$	-7.7×10^{-9}	$\Delta Q_z=\frac{R}{2\sqrt{\epsilon_z}}a_{27}$	-8.3×10^{-3}
Q Shift	$a_0=\frac{1}{\pi}\int_{-\pi}^{\pi}\beta_x d_x k'\,d\theta$	-2.4×10^{-5}	$\Delta Q_x=\frac{R}{4}a_0$	-6.2×10^{-3}
	$a_0=\frac{1}{\pi}\int_{-\pi}^{\pi}\beta_z d_x k'\,d\theta$	-3.0×10^{-5}	$\Delta Q_z=\frac{R}{4}a_0$	-7.7×10^{-3}
$2Q_z+Q_x=80$	$a_{80}=\frac{1}{\pi}\int_{-\pi}^{\pi}\beta_x^{1/2}\beta_z k'\cos 80\theta\,d\theta$	0.4096	$\Delta Q_x=-\frac{R}{16}\frac{\epsilon_z}{\sqrt{\epsilon_x}}a_{80}$	-8.9×10^{-3}
			$\Delta Q_z=\frac{R}{8}\sqrt{\epsilon_x}\,a_{80}$	3.56×10^{-2}
$2Q_z-Q_x=27$	$a_{27}=\frac{1}{\pi}\int_{-\pi}^{\pi}\beta_x^{1/2}\beta_z k'\cos 27\theta\,d\theta$	-3.0×10^{-6}	$\Delta Q_x=-\frac{R}{16}\frac{\epsilon_z}{\sqrt{\epsilon_x}}a_{27}$	6.5×10^{-8}
			$\Delta Q_z=\frac{R}{8}\sqrt{\epsilon_x}\,a_{27}$	-2.6×10^{-7}
$Q_z+Q_x=53$	$a_{53}=\frac{1}{\pi}\int_{-\pi}^{\pi}\beta_x^{1/2}\beta_z^{1/2}d_z k'\cos 53\theta\,d\theta$	5.77×10^{-5}	$\Delta Q_x=-\frac{R}{4}\sqrt{\frac{\epsilon_z}{\epsilon_x}}a_{53}$	-1.05×10^{-2}
			$\Delta Q_z=\frac{R}{4}\sqrt{\frac{\epsilon_x}{\epsilon_z}}a_{53}$	2.1×10^{-2}
$Q_z-Q_x=1$	$a_1=\frac{1}{\pi}\int_{-\pi}^{\pi}\beta_x^{1/2}\beta_z^{1/2}d_z k'\cos\theta\,d\theta$	-8.6×10^{-5}	$\Delta Q_x=-\frac{R}{4}\sqrt{\frac{\epsilon_z}{\epsilon_x}}a_1$	1.56×10^{-2}
			$\Delta Q_z=\frac{R}{4}\sqrt{\frac{\epsilon_x}{\epsilon_z}}a_1$	-3.12×10^{-2}

for each dipole of the HERA lattice, formed by persistent currents together with the chromaticity correcting sextupoles set to make the chromaticity zero in each plane.

Transport between these elements is described by a simple linear matrix whose parameters are determined by the betatron amplitudes and phases and dispersion associated with the non-linear elements. The matrix off-momentum particle will differ from that of the synchronous particle only in phase advance. No attempt is made to include the chromatic dependence of other betatron quantities though this might be studied by rerunning the program with a different data set. Much use was made of a facility which allows the user to impose Q values and a linear chromaticity coefficients irrespective of those implied by the data associated with the non-linear elements. In this way one may scan across a resonance to determine its width and investigate the effect of a chromatic Q spread.

An unusual feature of LIMATRA is that the effect of closed orbit distortion at the non-linear elements may be studied. The user specifies an r.m.s. closed orbit amplitude and before the tracking commences Monte-Carlo routine assigns a distortion to each element from a Gaussian distribution with the specified r.m.s. width. Each time the particle encounters an element it receives a kick, calculated from its position in the non-linear field including the closed orbit displacement. It is thought that the random selection of closed orbit amplitude, though it does not include the enhanced Fourier components close to the Q value to be expected in an uncorrected orbit, nevertheless simulates well the situation in a machine where the orbit has been corrected but imperfectly.

Another facility in the program is a partial simulation of synchrotron motion. By specifying a synchrotron frequency one can force the $\Delta p/p$ of the particle to oscillate with this frequency. Its Q value then follows this oscillation and in this way at least the numerology of synchro-betatron motion may be included. The simulation excludes the non-linear momentum dependence of the beta functions an approximation made deliberately to speed the tracking.

The program was modified to include random fluctuations in the strength of the persistent current sextupole fields among the magnets of the lattice.

Table 4 shows the widths of stop-bands found by single particle tracking with LIMATRA. The momentum error of the particle was zero and the imposed Q stepped to scan along a line normal to the stop-band. We assume that the particle is outside the stop-band if it survives 300 turns at a given Q value. The four resonances tabulated are those to be expected from a systematic pattern of sextupoles with four fold symmetry and the half integer stop-bands from the combined effect of closed orbit error within the sextupole pattern. Fig. 5 shows the places in the working diagram where these scans were made. We note that where we have compared LIMATRA widths with those calculated from Fourier analysis of the same sextupole pattern LIMATRA consistently sees a stop-band only half as wide. Despite exhaustive attempts to find the reason for this discrepancy including changing the initial particle phase, scanning over the resonance at other points along its length and a reexamination of the definitions of stop-band width, this factor two remains. If in doubt the reader is encouraged to assume that the effect of errors may be twice as strong as LIMATRA would have us believe, otherwise he may consider a factor 2 is perhaps as good an agreement as one may expect, bearing in mind that there are approximations in the Fourier analysis description.

We see from Table 4 that LIMATRA demonstrates the expected independence of the third order stop-bands on closed orbit amplitude while the half integer stop-bands show the expected linear dependence.

The pure horizontal ($3Q_H = 80$) stop-band is encouragingly narrow for a structure resonance but the skew resonance $Q_H + 2\,Q_V = 80$ which in the HERA report [4] is assumed to be no wider, turns out to be a nasty surprise being about 0.05 wide. In practice one would try to choose a Q value remote from such a structure resonance and this may be possible since HERA has a superperiodicity of 4. This means that the third integer systematic resonances are four times further apart in the Q diagram. Of course further study might reveal that an alternative Q value was close to a structure resonance of another order driven by an imperfection we have not included. We therefore persist in our study of the dynamics close to this resonance following the principle of clinging to the "devil we know" rather than falling under the influence of the "devil we don't".

However we did depart briefly from this working point to check the behaviour of a non-systematic third order resonance $3Q_H = 79$ driving by the random fluctuations in persistent currents around the bending magnets.

Table 4 : Resonance Widths Found by Simulation

Order		Closed orbit $x_{co} = z_{co}$ (mm)						***Fourier Analysis $x_{co} = z_{co} = 4$
		0	1	2	4	6	8	
$3Q_H = 80$	ΔQ_H	0.9×10^{-2}	0.8×10^{-2}	0.8×10^{-2}	0.8×10^{-2}	0.6×10^{-2}		1.97×10^{-2}
$2Q_V+Q_H = 80$	ΔQ_H	4.6×10^{-2} (3.3×10^{-2})*	4.6×10^{-2}	4.6×10^{-2}	4.2×10^{-2}	4.2×10^{-2}	4.2×10^{-2}	7.16×10^{-2}
	ΔQ_V	9.2×10^{-2} (6.6×10^{-2})*	9.2×10^{-2}	9.2×10^{-2}	8.4×10^{-2}	8.4×10^{-2}	8.4×10^{-2}	14.3×10^{-2}
$2Q_H = 53$	ΔQ_H		0.2×10^{-2}	0.8×10^{-2}	1.7×10^{-2}	2.4×10^{-2}	3.2×10^{-2}	4.76×10^{-2}
$2Q_V = 53$	ΔQ_V				3.0×10^{-2} ($<1\times10^{-3}$)**	5.5×10^{-2}	8.0×10^{-2}	3.14×10^{-2}

* Cross resonance at $Q_H = 26.79$, $Q_V = 26.61$

** Cross resonance at $Q_H = 26.30$, $Q_V = 26.50$

*** The projected resonance widths listed here are calculated using Guignard's[8] rigourous expressions

Table 5 shows that LIMATRA was only able to find the narrow resonance in the case where the zero harmonic persistent current sextupole was artificially suppressed to minimise the non-linear contributions to Q spread. In this case the width of the resonance is more than an order of magnitude smaller than its systematic counterpart. We conclude that the fluctuations of 10% among bending magnets with persistent current sextupole component does not significantly effect the dynamics of the machine.

The next part of the simulation study was aimed at exploring two regions of the working diagram which have proved in other machines with strong sextupoles [1) 2)] to be places where one can expect particle loss due to resonances to be minimal. We show the regions in Fig. 6 and label them NAL and SPS for historical reasons. At least at one time in the history of these machines they reflected their contrasting choice of working point.

Single particles were tracked for 1000 turns at each of the mesh points. The linear chromaticity imposed was zero and there were no synchrotron oscillations. Survival for 1000 turns with no sign of growths is indicated by a dot. A cross indicates that the particle became unstable and left the "machine".

Although the two regions appear to be of comparable extent we must remember that the closed orbit distortion assumed in the "NAL" region is 12 mm in each plane while in the "SPS" region it is only 5 mm. This adjustment was made to ensure a finite and comparable region of stability for both regions. (Both machines have of course corrected orbits which are much better than this).

We conclude that of the two regions bounded by the resonances which we assume are excited and by the coupling resonance the upper "NAL" one makes less stringent demands on closed orbit correction and is likely to be less critical from the tuning point of view than the "SPS" region. Note that unlike the SPS,HERA does not have to be tuned to the $Q_H = 26.66$ resonant for slow extraction.

Table 6 shows the result of a more detailed study of sensitivity to closed orbit distortion made with 100 particles at the centre of the SPS and NAL regions. The distribution of the 100 particles in phase space is within the emittances given in Table 1. At this stage synchrotron oscillations and random fluctuations among the persistent current sextupoles were not

Table 5 : Resonance Excited by Random Variation in Persistent Currents

No.	Order	Strength of sextupole				Fourier Analysis		LIMATRA Results	
		K'_{SF}	K'_{DF}	K'_{B}	$\Delta K'_{B}$	ΔQ_x	ΔQ_z	ΔQ_x	ΔQ_z
1	$3Q_H = 79$	0.2633	0.63907	-0.0107	0	3.147×10^{-5}		-	
2	$3Q_H = 79$	0.2633	0.63907	-0.0107	-0.00107	1.19×10^{-3}		-	
3	$3Q_H = 79$	0	0	0	-0.00107	1.19×10^{-3}		1.6×10^{-3}	
4	$Q_H+2Q_V = 79$	0.2633	0.63907	-0.0107	0	1.84×10^{-4}	3.68×10^{-4}	-	-
5	$Q_H+2Q_V = 79$	0.2633	0.63907	-0.0107	-0.00107	2.71×10^{-3}	5.42×10^{-3}	-	-
6	$Q_H+2Q_V = 79$	0	0	0	-0.00107	2.71×10^{-3}	5.42×10^{-3}	1.8×10^{-3}	3.6×10^{-3}

Table 6 : Tracking 100 Particles with Increasing Orbit Distortion

Working Point		Closed Orbit (mm)		The Number of Particles lost
Q_H	Q_V	x_{co}	z_{co}	
26.55	26.60	6	6	0
		7	7	0
		8	8	27
		8	0	0
		10	0	0
		0	8	100
		0	10	100
26.78	26.86	10	10	0
		12	12	2
		14	14	100
		14	0	0
		16	0	0
		0	14	100
		0	16	100

included. We see the NAL working point allows up to 12 mm distortion before a few particles begin to leave the machine, extracted by a nearby resonance. In the SPS case the threshold is below 8 mm and surprisingly is lower if the horizontal orbit is perfect. In both cases it is the effect of vertical distortion which is more critical.

Table 7 shows first the effect of a momentum spread in a machine with an unbalanced chromaticity. The momentum oscillates with a synchrotron frequency corresponding to HERA's $Q_s = 8.6\times10^{-3}$ at injection. The momentum spread is $\pm1.6\times10^{-3}$, again simulating HERA at 40 GeV.

We see that if the closed orbit distortion is zero the linear chromaticity threshold is as high as 0.6 but mixing in 2 mm of random orbit distortion severely restricts the range of stable chromaticity to 0.1 or lower. In the last part of the Table we show how it is indeed the edge of the momentum spread which is extracted in the case where the chromaticity is 0.1 and there is 2 mm of distortion.

In practice, as in the SPS, a finite linear chromaticity of about 0.1 will be needed in HERA to stabilise the head-tail and multibunch instabilities and it is unlikely that operationally the orbit can be corrected to much better than 1 or 2 mm r.m.s. at injection. We see that under these conditions the edge of the HERA momentum spread leaves the machine in less than 22 milliseconds. While it might be expected that once this tail has been extracted the rest of the beam will remain in the machine perhaps even for the half hour or so necessary to fill HERA we are unable to test this conjecture within the practical limitations of even modern fast computing resources. Because each non-linear element must be simulated, one particle turn takes 10 msec and simulating 100 particles for 22 msec (1000 turns) uses 15 minutes of CDC 7600 times. Faster computers and more efficient coding might extend our multiparticle simulation to perhaps a second or so of HERA time but never to a quarter of an hour. We have tracked a single particle with $\Delta p/p = 1.0\times10^{-3}$ corresponding to the fourth line of Table 7 and with a two standard deviation betatron amplitude for 10 seconds of HERA time without loss but this may have had favourable initial coordinates.

Table 7 : Tracking 100 Particles as a Function of Chromaticity and $\Delta p/p$

Momentum spread $\frac{\Delta p}{p}$	Closed Orbit (mm)		Chromaticity $\xi = \frac{\Delta Q/Q}{\Delta p/p}$	Number of particles lost
	x_{co}	z_{co}		
1.6×10^{-3}	0	0	0.4	0
			0.5	0
			0.6	1
1.6×10^{-3}	1	1	0.2	0
			0.3	0
			0.4	1
1.6×10^{-3}			0.001	0
			0.01	0
			0.025	2
1.0×10^{-3}	2	2	0.1	0
1.2×10^{-3}	2	2	0.1	0
1.4×10^{-3}	2	2	0.1	1
1.6×10^{-3}	2	2	0.1	2

We are forced to conclude that while simulation has confirmed the influence of persistent current sextupoles on the dynamics and demonstrated the existence of stable regions in the Q diagram, the sensitivity of the beam survival to tuning suggests that we shall have to radically reduce the effect of persistent currents if HERA's beam is to remain circulating at 40 GeV for 15 minutes or so.

6. IMPROVEMENTS OF HERA

Raising the injection energy to that of the Energy Doubler would no doubt help a lot but would involve the construction of a 150 GeV conventional proton machine and we rule it out.

Moving to a Q which is remote from the structure resonance will probably not help, though clearly a simulation of this should be the next step. The structure resonance does not at first sight seem to be the principal reason for the restriction on closed orbit and chromaticity for we have confirmed that the structure resonance itself is orbit independent.

One may also explore the implication of raising Q to be between 30 and 40 since we have seen that moving from a machine with Q close to 19 to a Q close to 26 considerably reduces the chromaticity due to sextupole imperfection.

Another avenue of study may lie in the direction of deviding sextupoles into more families to linearise the chromaticity but since LIMATRA does not include many of the non-linear effects the additional families correct, this would not seem to be a way of extending the tolerance of the machine to linear chromaticity.

Perhaps a marginal situation might be improved by a combination of such measures but before we can be sure that the particles which survive the first 1000 turns of our simulation will live to collide with electrons then must be a radical improvement in the persistent current situation.

We therefore suggest that we make use of the fact that by following a particular trajectory in Fig. 3. one can end up at 40 GeV with a mean sextupole field which is zero. The random fluctuations (about one tenth of the persistent field assumed above) will remain but hopefully the worst effects of closed orbit error combined with sextupole field will disappear. We intend to simulate this situation in the next round of our studies.

To end on a hopeful note we point out that we have, in the ideal situation in which HERA is precisely tuned and there there are no other undesirable dynamic effects, found stable dynamic conditions. The improvements are needed because we suspect in practice it will be difficult to reach this ideal situation

REFERENCES

1) R. Stiening and E.J.N. Wilson, Nuclear Instrum. Methods 121, p 275 (1974).

2) M. Cornacchia, R. Lackner, W. Mills, R. Stiening, G. von Hotley, E.J.N. Wilson. IEEE Trans. on Nuc. Sci., Vol NS-24, No. 3, p. 1482 (1977).

3) A Report on the Design of the FNAL Superconducting Accelerator. FNAL Design Report, May 1979.

4) Study on the Proton-Electron Storage Ring Project HERA, DESY HERA 80/01.

5) M. Cornacchia. CERN Lab. II DI-PA/Int. 75-8.

6) G. von Holtey. CERN Lab. II DI-PA/Int. 75-3.

7) E. Keil, Y. Marti, B.W. Montague and A. Sudboe. CERN 75-13.

8) G. Guignard. CERN 70.24.

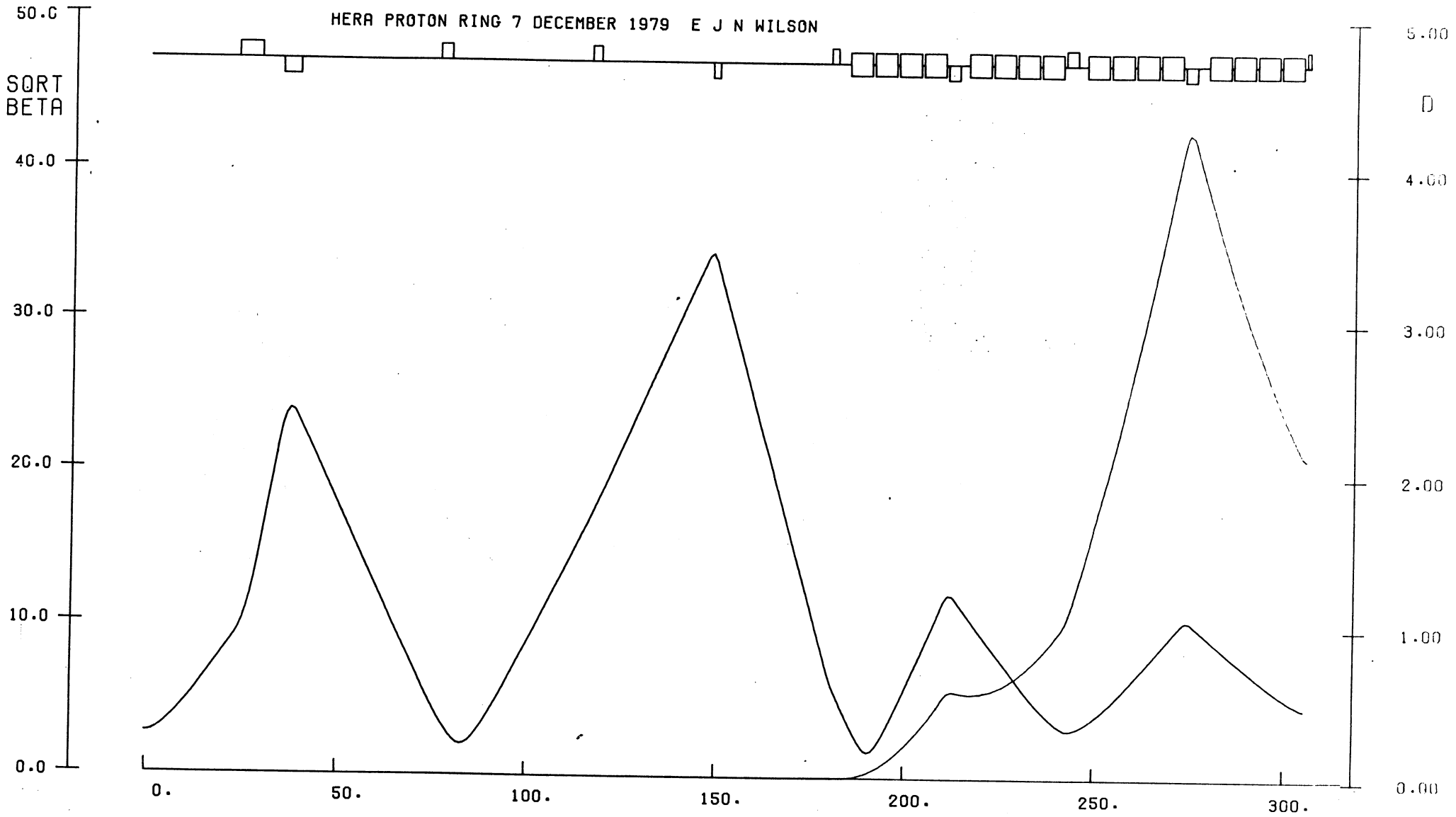

Fig. 1 Low Beta Insertion from Crossing Point to Beginning of the Arc

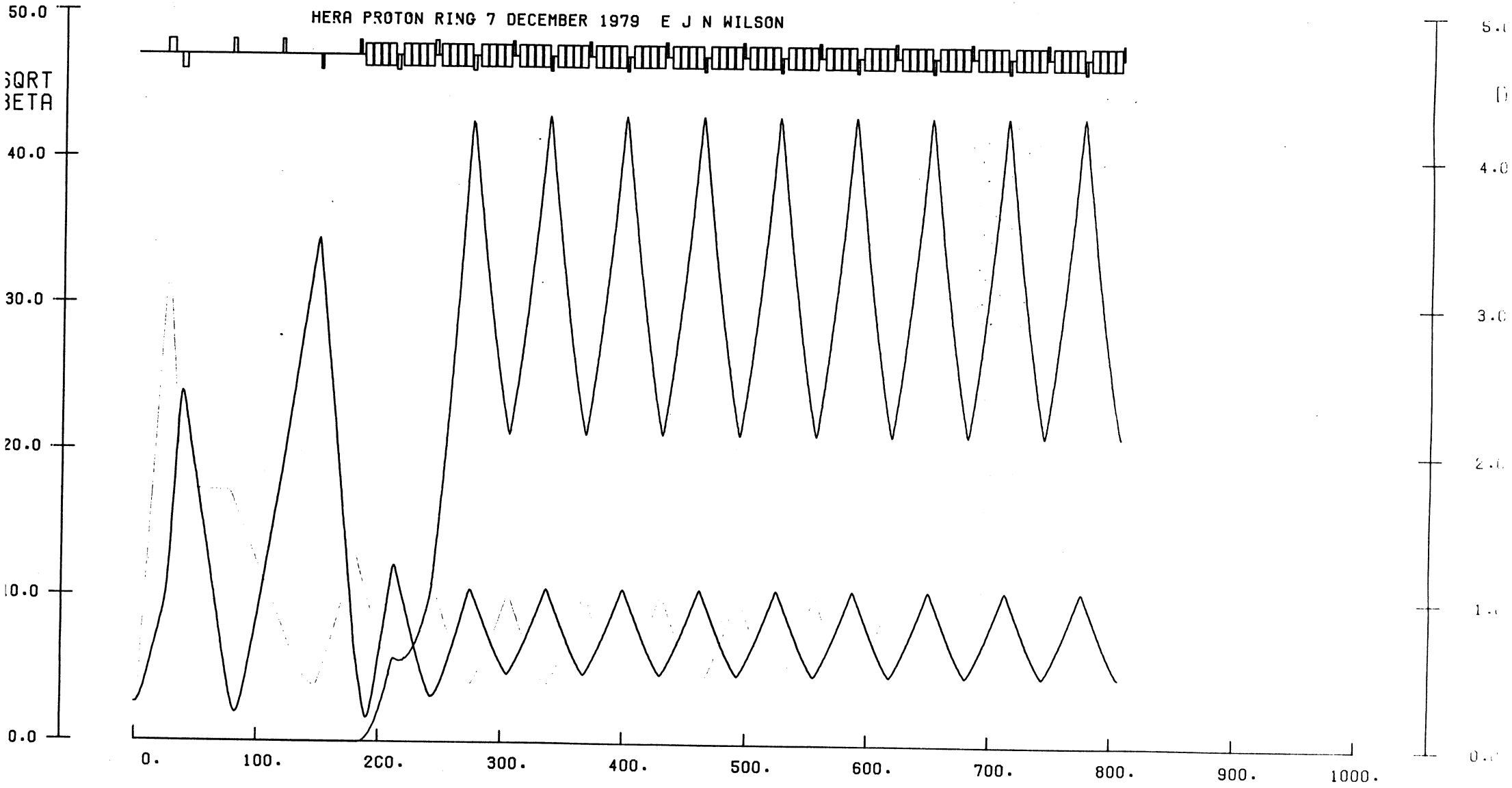

Fig. 2 One Half Superperiod (1/8th) of HERA from Crossing Point

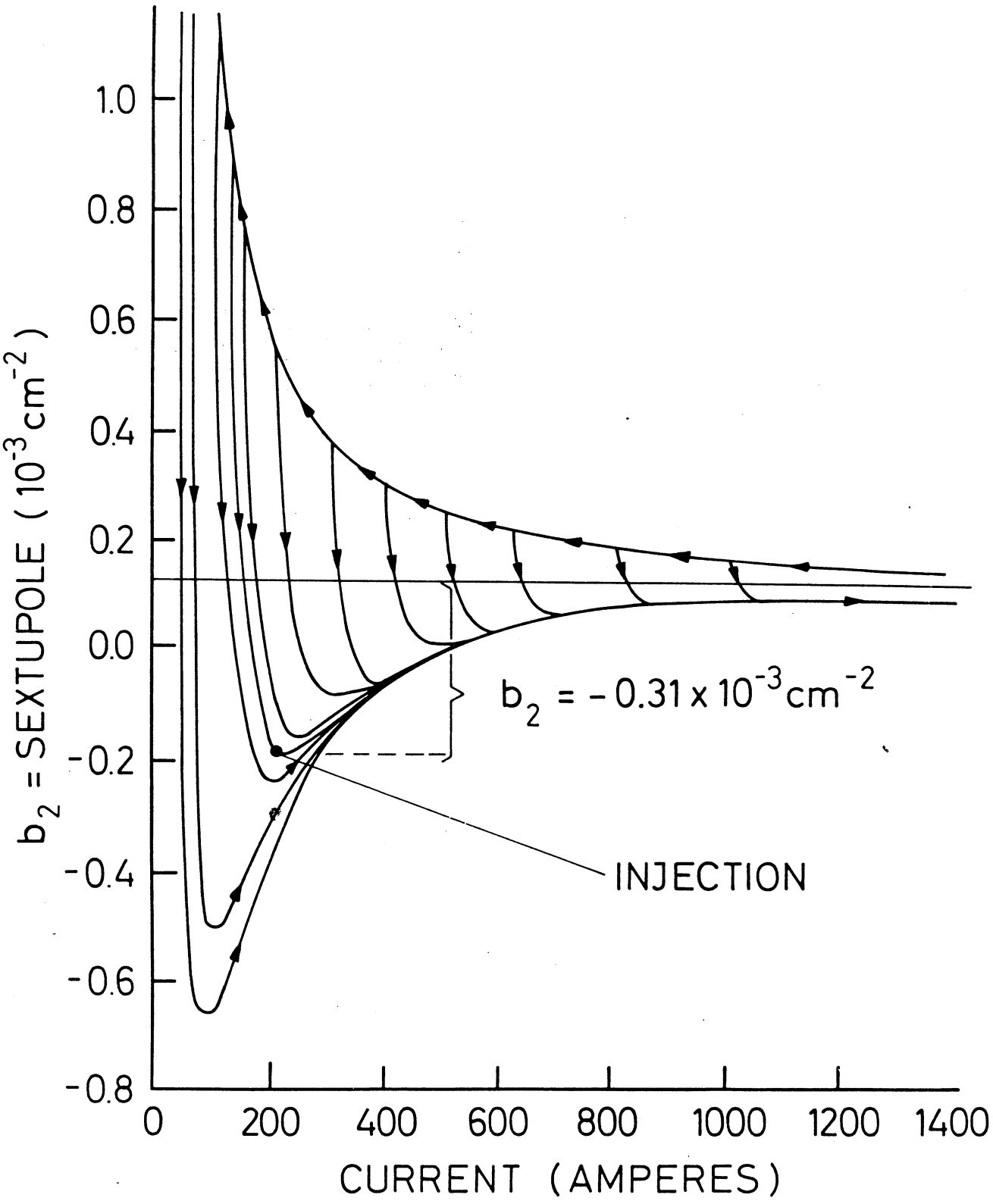

Fig. 3 Persistent Current Sextupole in a Dipole Magnet

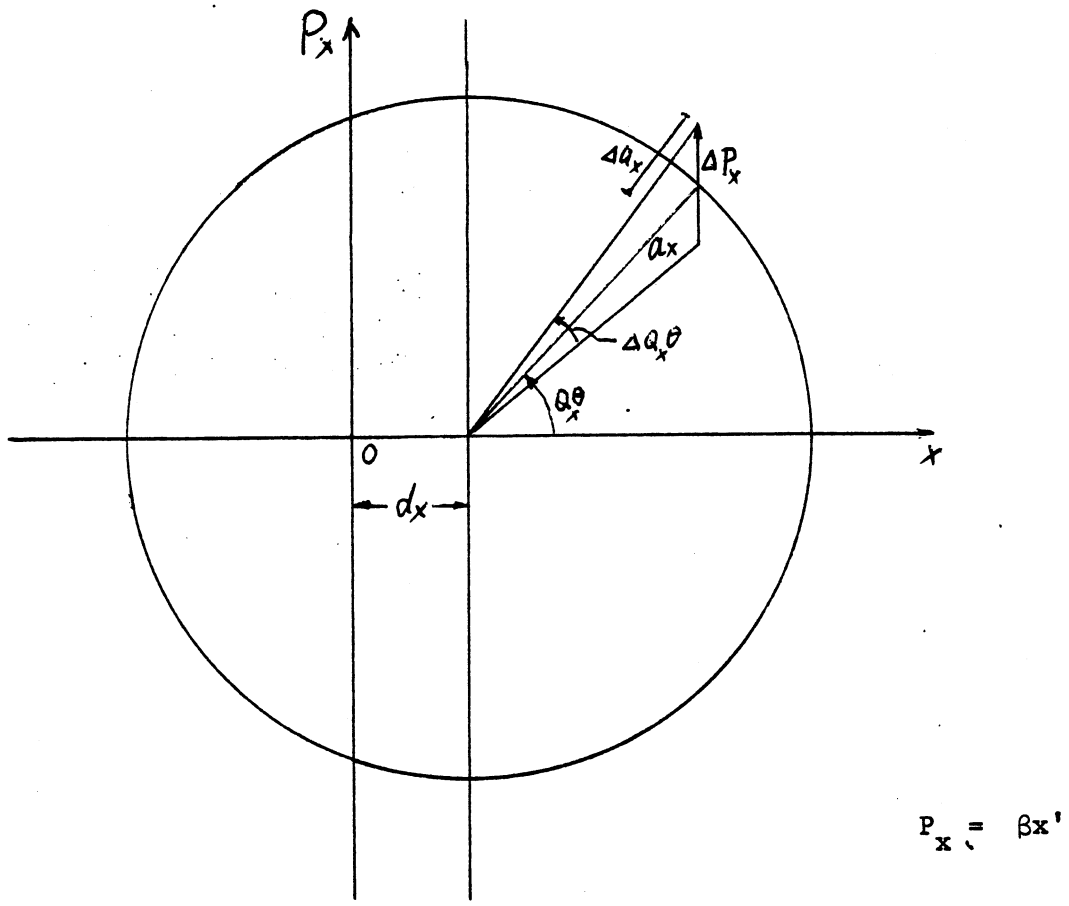

Fig. 4 Circle Diagram shows Effect of a Sextupole on a Beam Displaced by Closed Orbit Distortion.

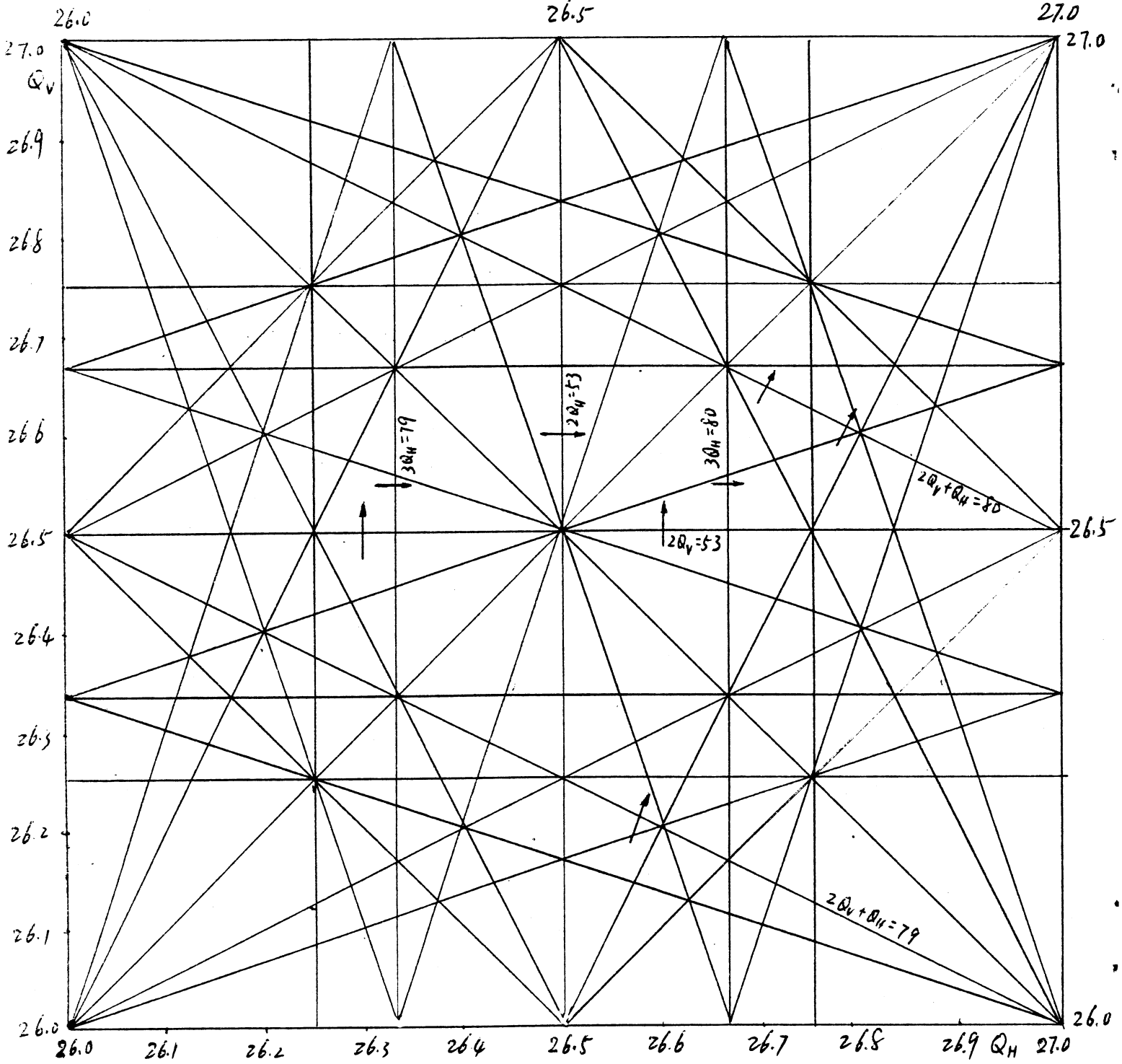

Fig. 5 Q Diagram Showing the Places Where Scans Were Made. Indicated by Arrows

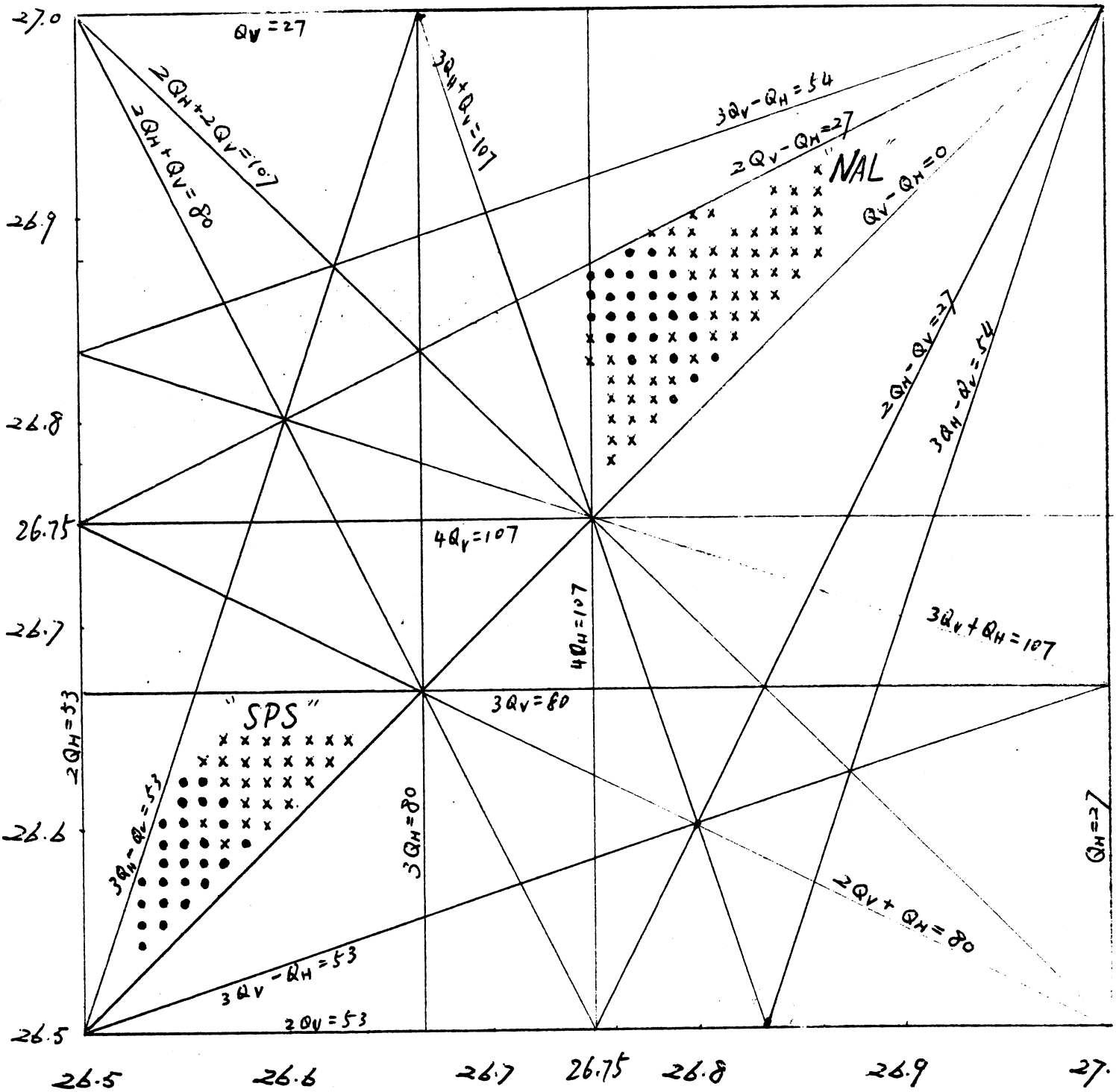

Fig. 6 Q Diagram Showing Regions in which the Simulation Gave Stable and Unstable Tracking

(. = 1000 turns survival, x = particle lost in < 1000 turns)